



Article

CASPT2 Potential Energy Curves for NO Dissociation in a Ruthenium Nitrosyl Complex

Francesco Talotta ^{1,2,3}, Leticia González ^{3,4}  and Martial Boggio-Pasqua ^{2,*} 

¹ Institut de Chimie et Physique, UMR 8000 CNRS/Université Paris-Saclay, 91405 Orsay, France; francesco.talotta@universite-paris-saclay.fr

² Laboratoire de Chimie et Physique Quantiques, IRSAMC, CNRS/Université Toulouse 3, 118 route de Narbonne, 31062 Toulouse, France

³ Institut für Theoretische Chemie, Fakultät für Chemie, Universität Wien, Währinger Strasse 17, 1090 Vienna, Austria; leticia.gonzalez@univie.ac.at

⁴ Vienna Research Platform on Accelerating Photoreaction Discovery, Universität Wien, Währinger Strasse 17, 1090 Vienna, Austria

* Correspondence: martial.boggio@irsamc.ups-tlse.fr; Tel.: +33-561-556-833

Academic Editor: Dereck J. Mcphee

Received: 12 May 2020; Accepted: 2 June 2020; Published: 4 June 2020



Abstract: Ruthenium nitrosyl complexes are fascinating photoactive compounds showing complex photoreactivity, such as N→O linkage photoisomerism and NO photorelease. This dual photochemical behavior has been the subject of many experimental studies in order to optimize these systems for applications as photoswitches or therapeutic agents for NO delivery. However, despite recent experimental and computational studies along this line, the underlying photochemical mechanisms still need to be elucidated for a more efficient design of these systems. Here, we present a theoretical contribution based on the calculations of excited-state potential energy profiles for NO dissociation in the prototype *trans*-[RuCl(NO)(py)₄]²⁺ complex at the complete active space second-order perturbation theory (CASPT2). The results point to a sequential two-step photon absorption photorelease mechanism coupled to partial photoisomerization to a side-on intermediate, in agreement with previous density functional theory calculations.

Keywords: photorelease; photoisomerization; photochromism; computational photochemistry; ab initio calculations

1. Introduction

Ruthenium nitrosyl complexes have attracted considerable interest over the last decades because of their multifunctional photoresponsive capability. Indeed, these complexes can display photochromism in the solid state [1–15] and be efficient agents for NO photorelease in solution [16–30]. Despite the numerous studies exploiting these two distinct photoreactivities (i.e., N→O linkage photoisomerization and photoinduced NO delivery), the underlying mechanisms are notoriously complex to unravel based on the available experimental observations [12,30].

Computational photochemistry has proven to be a highly efficient tool to understand photo-induced molecular processes [31]. Although a vast majority of computational studies are dealing with organic photochemistry [32–35] due to the difficulty of computing photochemical pathways in metal complexes [36], recent computational investigations of photoisomerizable metal complexes have been published with the aim of understanding their photoswitching mechanisms [37–45]. Regarding ruthenium nitrosyl complexes, the N→O linkage photoisomerization mechanism in the *trans*-[RuCl(NO)(py)₄]²⁺ (where py denotes a pyridine ligand) complex was investigated using density functional theory (DFT) and multi-state complete active space second-order perturbation theory

(MS-CASPT2) to calculate the lowest singlet and triplet potential energy surfaces [43–45]. These studies revealed an activated and energetically uphill process in the lowest triplet excited state, which forbids a simple adiabatic mechanism in this electronic state, and suggested a complex sequential two-step photon absorption mechanism involving nonadiabatic processes (Figure 1). This mechanistic picture was later confirmed experimentally [12]. The proposed photoisomerization mechanism can be summarized as follows: upon blue-light absorption, the initial ground-state N-bonded (η^1 -N) species, GS, undergoes a partial isomerization to the η^2 -NO side-on metastable state MS2 following various internal conversions and intersystem crossings. This key intermediate then absorbs a second blue-light photon under continuous irradiation to produce the final N→O linkage isomer corresponding to the O-bonded (η^1 -O) isonitrosyl form, denoted MS1.

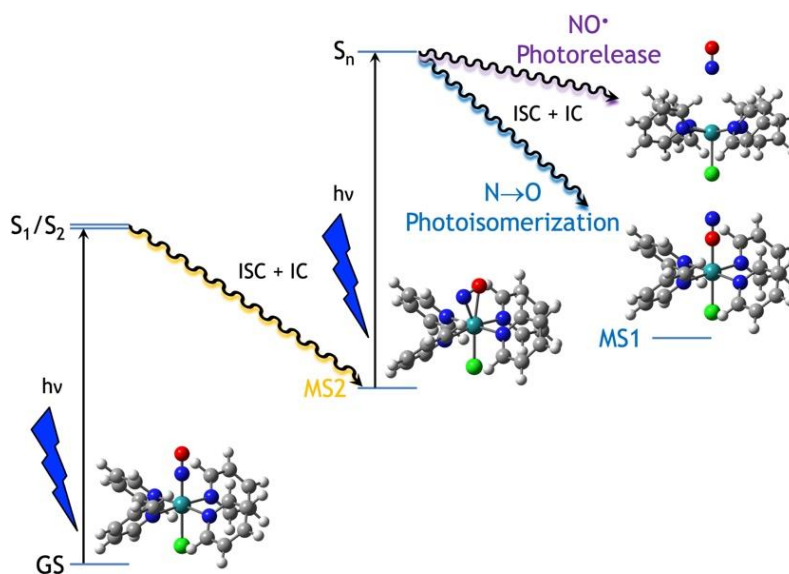


Figure 1. Scheme illustrating the competitive and intricate N→O linkage photoisomerization and NO• photorelease mechanism in the *trans*-[RuCl(NO)(py)₄]²⁺ complex. ISC: intersystem crossing. IC: internal conversion.

In addition to their ability to undergo linkage photoisomerizations, ruthenium nitrosyl complexes can also release nitric oxide upon light irradiation. The mechanism for NO• photorelease is important, as this radical is involved in various physiological and pathological processes [46] and ruthenium nitrosyl complexes can be designed to promote NO• photorelease, in particular using low-power light for biological and medicinal applications [24,26,29,47,48]. Experimental studies in the solid phase have shown that the photoproducts of both N→O linkage photoisomerization and NO• photorelease could be observed, suggesting that weakly bound linkage isomers of nitric oxide are likely intermediates in the photolytic release of NO• [19,22]. Very few theoretical studies have been devoted to NO• photorelease. The initial stages of NO• photorelease was investigated dynamically for the [Ru(PaPy₃)(NO)]²⁺ complex (where PaPy₃ = *N,N'*-bis(2-pyridylmethyl)amine-*N*-ethyl-2-pyridine-2-carboxamide) [49]. However, no excited-state intermediate could be identified as key transient species in the NO• photorelease from these simulations. Later, a static DFT study investigating the lowest triplet potential energy surfaces of different ruthenium nitrosyl complexes identified a triplet η^2 -NO side-on structure denoted ³MS2, as the key intermediate for NO• photorelease [50]. This finding suggested that partial photoisomerization to the η^2 -NO side-on MS2 metastable state was at least required for NO• photorelease and that a sequential two-step photon absorption mechanism was involved like in the photoisomerization process (Figure 1). Soon after, a complete active space self-consistent field (CASSCF)-in-DFT embedding approach was used to explore the ground and excited electronic states of the *trans*-[RuCl(NO)(NH₃)₄]²⁺ complex along the Ru–NO stretching normal mode [51]. However, vibrational relaxation in the excited

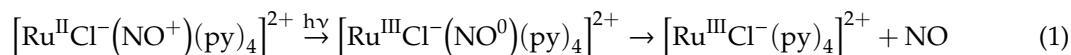
states was not taken into account and no information on the intermediates responsible for the NO• photorelease was provided in that study.

The *trans*-[RuCl(NO)(py)₄]²⁺ has often served as a prototype ruthenium nitrosyl system to study both N→O linkage photoisomerization and NO• photorelease because of its capability to undergo both photoreactivities [9–12,52]. In this article, we present the results of accurate multireference ab initio CASPT2 calculations along NO• photodissociation pathways in order to verify the validity of the DFT mechanistic picture previously reported [50] on this complex and to identify the most likely intermediate for NO• photorelease. These results reveal further insight into how photorelease and photoisomerization are interconnected for this prototypical molecule.

2. Results and Discussion

2.1. Previous DFT Results of NO Photodissociation

The main mechanistic assumptions for the determination of the NO• photorelease pathways is that i) this process occurs from the lowest triplet excited states, as suggested by the rapid population of these states after initial irradiation and ultrafast intersystem crossing (ISC) [45,49,53], and that ii) it involves initially a decoordination of the NO• radical [19,22]. According to i), three triplet-state intermediates (Figure 2) were located on the lowest triplet potential energy surface at the DFT level [43,44,50]. The lowest energy intermediate is a triplet N-bonded (η^1 -N) species denoted ³GS, in which the Ru–N–O is bent, unlike the structure of the initial N-bonded GS that presents a collinear Ru–N–O alignment. Another triplet intermediate is the η^2 -NO side-on structure ³MS2 mentioned above. The third triplet state corresponds to an O-bonded (η^1 -O) species denoted ³MS1, in which the Ru–O–N is also bent, whereas it is collinear in the singlet MS1. All these intermediates are potential candidates for transient species in the NO• photorelease mechanism. Thus, a straightforward computational strategy consists in calculating the dissociation energy of NO• from these triplet excited-state species. If we write formally the chemical equations for the photorelease pathway—note that the triplet excited states ³GS, ³MS2 and ³MS1 all have a dominant MLCT character [43]—the ruthenium center can be written formally as Ru^{III} and one could postulate:



Although we know that it is not possible to assign such clear formal oxidation states to these species [54], it allows us to have a simple chemical representation of the expected fragments. From Equation (1), the Ru–NO photodissociation should produce two doublet states (radicals): one corresponding to a pentacoordinated ruthenium complex and one corresponding to nitric oxide.

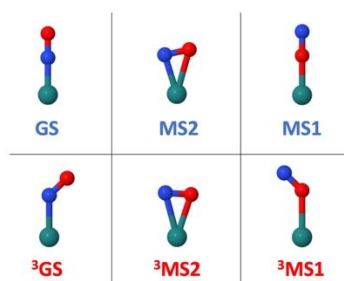


Figure 2. Illustration of the Ru–N–O geometrical arrangement in the singlet ground-state structures (GS, MS2, MS1) and in the triplet excited-states intermediates (³GS, ³MS2, ³MS1). Color code: Ru in cyan, N in blue and O in red.

DFT potential energy profiles for the NO• photorelease pathways of the *trans*-[RuCl(NO)(py)₄]²⁺ complex are reproduced in Figure 3 from Ref. [50]. They are based on the use of the B3LYP-D3 functional to calculate minimum energy paths along the NO dissociation from the three triplet excited

states 3GS , 3MS2 and 3MS1 . They show that the 3MS2 intermediate is the one that requires less energy to dissociate Ru–NO, in agreement with the fact that the 3MS2 intermediate is the highest energy triplet-state intermediate at this level of theory [43,50]. However, these energy profiles also reveal a wrong physical behavior at the asymptotic limit, as the energy is still substantially decreasing when the Ru–NO distance is increasing beyond 9 Å. According to Equation (1), the expected spin densities of the fragments produced should be exactly equal to 1. However, at the B3LYP-D3 level of theory, these spin densities are 1.2 and 0.8, for $[Ru^{III}Cl^-(py)_4]^{2+}$ and NO^\bullet , respectively, indicating an artificial electron (charge) transfer between the NO^\bullet and $[Ru^{III}Cl^-(py)_4]^{2+}$ fragments. In addition, the NO^\bullet radical has a doubly degenerate $X^2\Pi$ ground state, which cannot be physically described with a single-configuration representation of the DFT wavefunction. Thus, we report next CASPT2 potential energy curves for NO^\bullet dissociation which address both issues.

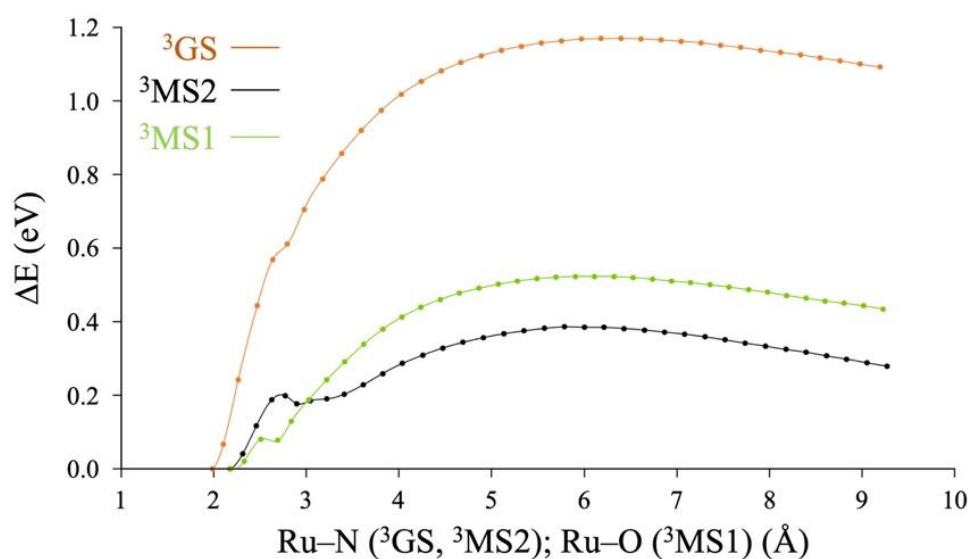


Figure 3. Minimum energy paths for NO dissociation in the *trans*- $[RuCl(NO)(py)_4]^{2+}$ complex at the B3LYP-D3 level of theory from the three triplet excited states 3GS , 3MS2 and 3MS1 . The zero energy is set to the triplet energy of the 3GS , 3MS2 and 3MS1 at their respective minima for each curve. Adapted with permission from Ref. [50].

2.2. CASPT2 Results of NO Photodissociation

The deficiencies of DFT can be overcome using CASPT2 to compute the Ru–NO photodissociation potential energy profiles starting from each intermediate. The results of the CASPT2 calculations are represented in Figure 4. The first obvious outcome of these calculations is that the lowest pair of singlet states S_0/S_1 and the lowest pair of triplet states T_1/T_2 all dissociate correctly to the same asymptote. Figure 4a,b shows that the complex dissociates to $[RuCl(py)_4]^{2+} + NO^\bullet$, with the pentacoordinated complex bearing its unpaired electron in the d_{xz} orbital of the Ru center, while NO^\bullet has its unpaired electron either in a π_x or π_y orbital. Of course, the two doublet states of the dissociated fragments can be spin-coupled in a singlet or in a triplet state without changing the asymptotic limit. For the same reason, the next two pairs of singlet and triplet states are also degenerate between each other: S_2/S_3 and T_3/T_4 dissociate to an excited state of $[RuCl(Py)_4]^{2+} + NO^\bullet$ with the metal fragment bearing its unpaired electron in the d_{xy} orbital of the Ru center and NO^\bullet in its doubly degenerate $X^2\Pi$ state. Finally, the third pair of singlet states S_4/S_5 is degenerate with T_5/T_6 , where the complex is now having its unpaired electron in the d_{yz} orbital of the ruthenium.

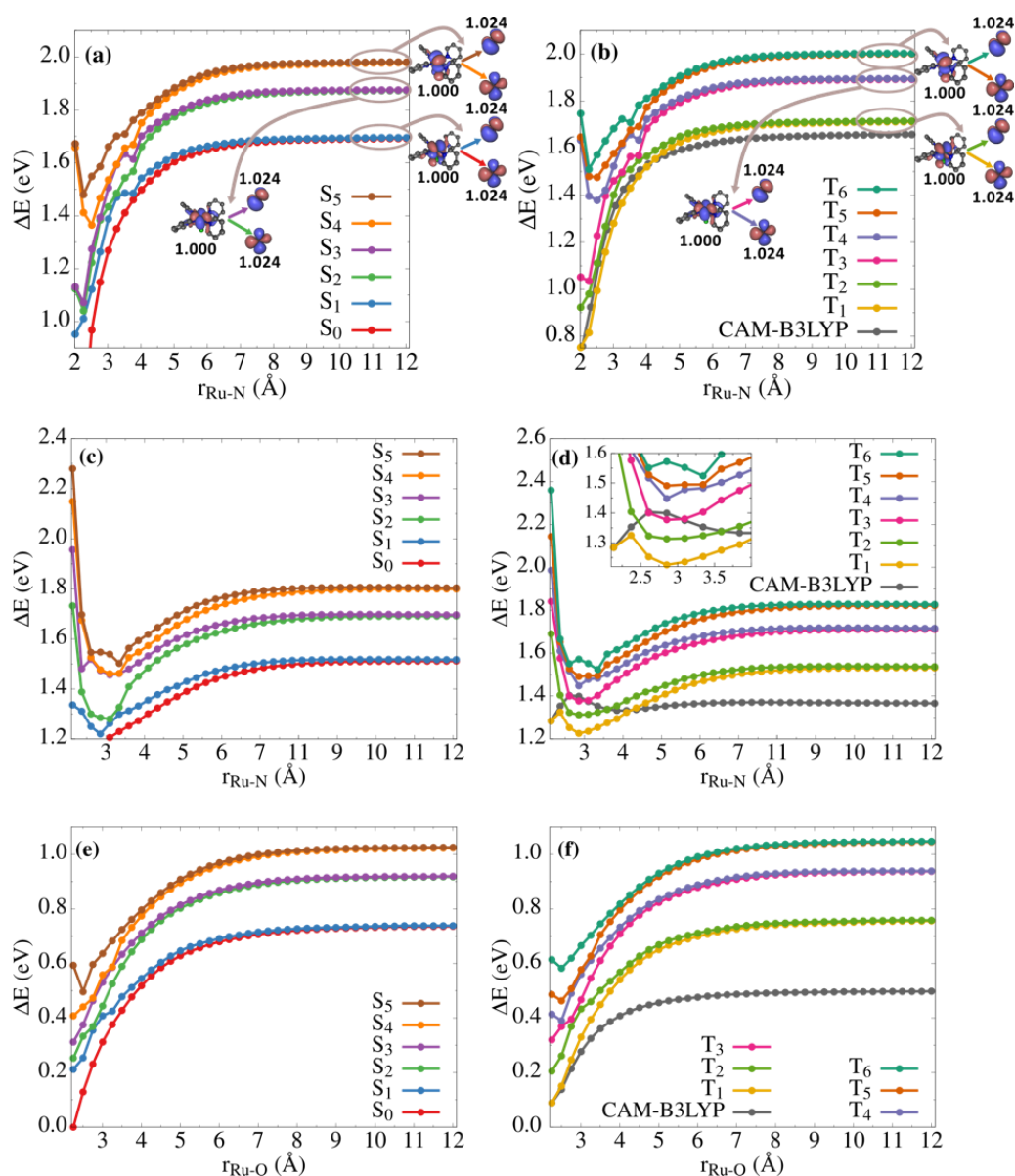


Figure 4. CASPT2 potential energy profiles along the Ru–NO or Ru–ON photodissociation for singlet states (**a,c,e**) and triplet states (**b,d,f**). Top, middle and bottom panels refer to photodissociation from 3GS , 3MS2 and 3MS1 , respectively. The zero energy is set to the S_0 electronic state. The CAM-B3LYP result is shown in (**b,d,f**) for each isomer. The hole/particle CASSCF molecular orbitals are also shown for each pair of degenerate states at the asymptotic limit along with their state-specific occupation numbers indicated in bold.

It is important to note that these CASPT2 potential energy profiles are computed on the structures resulting from relaxed scans performed on the lowest triplet T_1 state at the DFT level (see Computational Details). Given that B3LYP-D3 cannot describe the correct electronic structures at the asymptotic limit, we used CAM-B3LYP, which does not suffer from the artificial charge transfer problem between the dissociated fragments observed with B3LYP-D3, and thus provides the expected spin densities of 1.0 for the metal complex and the NO^\bullet fragments and the correct asymptotic behavior (see Figure 4). Thus, assuming that CAM-B3LYP provides reasonable structures along these scans, the CASPT2 potential energy profiles for the T_1 state shown in Figure 4b,d,f provide a reliable representation of the minimum energy paths for the photodissociation in the lowest triplet excited state from 3GS , 3MS2 and 3MS1 ,

respectively. Note also that the relaxed pentacoordinated complex presents a C_2 symmetry resulting from Jahn-Teller effects, that break the C_4 symmetry of the doubly-degenerate E state.

The photodissociation from 3GS shown in Figure 4b illustrates that there is a fairly good agreement between the CAM-B3LYP and CASPT2 potential energy profiles with dissociation energies of 0.91 eV and 0.96 eV, respectively, and smooth dissociation curves (weak state coupling). In contrast, for 3MS2 and 3MS1 (Figure 4d,f), the situation is very different with substantial deviations between the CAM-B3LYP and CASPT2 curves. While CAM-B3LYP predicts dissociation energies of 0.08 eV and 0.41 eV, respectively, the corresponding values at the CASPT2 level are 0.25 eV and 0.67 eV. In addition, Figure 4d shows a complex picture for the photodissociation curves from 3MS2 with many crossings occurring between the lowest triplet states including T_1 . In particular, a local potential energy well is created on the T_1 potential energy surface at a Ru–N distance of about 2.8 Å due to a T_1/T_2 crossing. It is worth noting that this minimum is also visible at the B3LYP-D3 level (Figure 3) and at the CAM-B3LYP level (Figure 4d), and is also associated with a change of the electronic configuration in the unrestricted Kohn-Sham solution. At the CASPT2 level, this secondary minimum even appears lower in energy than that of 3MS2 , which would need to be confirmed by geometry optimizations at the CASPT2 level beyond our available computational resources for such a large system.

Overall, it is encouraging that, while the energetics are quantitatively different between the DFT and CASPT2 methods, the qualitative behavior between the two approaches is similar and the intermediate triplet species predicted to have the lowest Ru–NO dissociation energy is 3MS2 , in agreement with the previous DFT study [50]. The dissociation energy curves on the singlet states are provided in Figure 4a,c,d for the sake of comparison, although photodissociation from the singlet excited states is less likely considering the efficiency of ISC in this type of systems after initial irradiation [45,49,53]. Note also that the lowest-energy dissociation path on S_0 would follow a very different pathway from the ones shown in Figure 4, as it would involve dissociation to $[Ru^{II}Cl^-(py)_4]^+ + NO^+$.

3. Computational Details

The CASPT2 approach was used to describe the potential energy surfaces of the singlet ground state and lowest triplet excited states along the Ru–NO photodissociation pathways. Because of the issues described above with the B3LYP-D3 energy profiles, we have used the geometries coming out from relaxed scans along the Ru–N or Ru–O bond distances using the CAM-B3LYP functional [55]. The scans were started from 3GS , 3MS2 and 3MS1 structures optimized with CAM-B3LYP and the def2-TZVP basis set [56] on all atoms and the associated small-core relativistic pseudopotential for the Ru center [57]. These scans were performed at the same level of theory stepping along the Ru–N distance from 3GS and 3MS2 , and along the Ru–O distance from 3MS1 . The orientation of the departing NO was constrained by freezing some relevant angles during the scan.

The active space chosen for the underlying reference CASSCF calculations is shown in Figure 5 for the 3GS configuration and at its dissociation limit. A distribution of 14 electrons within 10 orbitals (i.e., CASSCF(14,10)) has been employed. The active space (active orbitals) is constituted of the main orbitals involved to describe the photodissociation process. The three occupied Ru(4d) valence orbitals correlating with the t_{2g} orbitals were included. The two e_g orbitals (d_{z^2} and $d_{x^2-y^2}$) does not appear to be involved in the NO dissociation. Two pairs of π and π^* and the pair of σ and σ^* orbitals of NO were also included, plus a $\sigma^*(2s)$. More extended active spaces have been tested, notably including the Ru($4d_{x^2-y^2}$) orbital and N(2p) orbitals of the equatorial pyridine ligands. Nevertheless, the CASSCF(14,10) proved to be the most stable with the proper asymptotic degeneracy expected for three consecutive pairs of singlet and triplet excited states (vide supra). Note that in linear configurations (e.g., like in GS and MS1), the $4d_{z^2}$ also overlaps with the σ orbital [45], which does not appear to be the case when the Ru–N–O is bent (e.g., like in 3GS , 3MS2 and 3MS1).

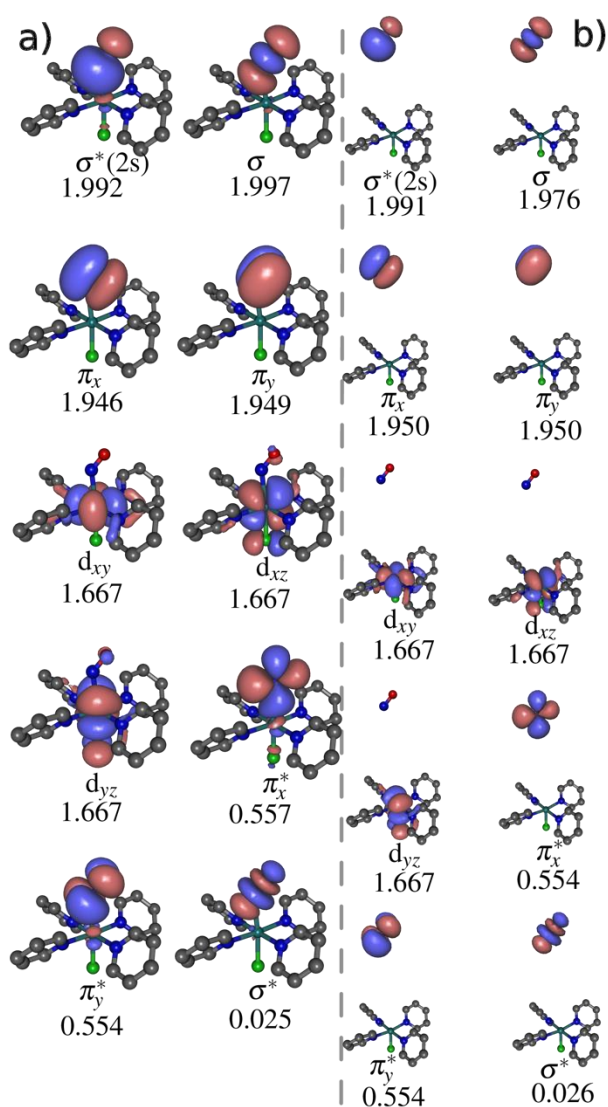


Figure 5. SA6-CASSCF(14,10) active space orbitals for the ^3GS isomer, and their respective average occupation numbers for the triplet states (a) at the ^3GS minimum and (b) at the asymptotic region.

The CASSCF calculations were performed averaging over 6 states for each spin state (singlet and triplet), in order to obtain good asymptotic behavior (degeneracies of pairs of electronic states due to the doubly-degenerate $X^2\Pi$ state of NO^\bullet) of the potential energy surfaces at the dissociation limit. For the same reason, multi-state CASPT2 (MS-CASPT2) was executed over 6 states. However, the MS-CASPT2 calculations proved to be extremely unstable at the asymptotic region because of artificial state mixing breaking the degeneracy of the doubly-degenerate $X^2\Pi$ state of NO^\bullet . This is a well-known issue of MS-CASPT2, which can occur when the electronic states are nearly or exactly degenerate [58]. Accordingly, only the state-specific CASPT2 (simply labelled as CASPT2) excited-state energies are reported in this study.

All the CASSCF and CASPT2 calculations were performed with the OpenMolcas program package [59], using the Cholesky decomposition algorithm with a threshold of 10^{-6} a.u. and the ANO-RCC-VTZP all-electron basis for Ru [60] and ANO-RCC-VDZP for all other atoms [61]. This precision in the two-electron integrals was required to solve degeneracy issues at the dissociation asymptotic region. A level shift of 0.3 a.u. and a standard IPEA shift [62,63] of 0.25 a.u. were used to run the CASPT2 calculations. The DFT calculations were performed with Gaussian 09 [64].

4. Conclusions

We report, in this work, accurate CASPT2 potential energy profiles of the lowest six singlet and six triplet states along the most probable photodissociation pathways of NO• in the prototype *trans*-[RuCl(NO)(py)₄]²⁺ complex. These calculations were performed from the three lowest triplet excited state intermediates previously identified in DFT studies [43,44,50]. By choosing an appropriate active space and treating several pairs of singlet and triplet states simultaneously, we address correctly the bond dissociation process and the degeneracies between the electronic states at the asymptotic limit.

Our results support the conclusion of a previous DFT study [50], which predicted the ³MS2 intermediate to be the most likely candidate for NO• photorelease. Further, we report a dissociation energy from the triplet ³MS2 intermediate of only 0.25 eV, which is 0.71 eV and 0.42 eV lower than that from ³GS and ³MS1, respectively. Because population of this intermediate requires absorption of a second photon from MS2, the proposed mechanism for photorelease is that it is coupled to partial photoisomerization through a sequential two-step photon absorption mechanism. Because ³MS2 is also a key excited-state intermediate in the N→O linkage photoisomerization mechanism [43–45] leading to MS1, this triplet side-on species is possibly the branching structure on the lowest triplet potential energy surface for the two competing photochemical pathways: N→O linkage photoisomerization and NO• photorelease.

Author Contributions: F.T. performed all the calculations, participated in the interpretation of the results and in the manuscript preparation. L.G. and M.B.-P. conceived the project, were involved in the interpretation of the results and manuscript preparation. All authors have read and agreed to the published version of the manuscript.

Funding: This research was funded by the European Union's Horizon 2020 research and innovation programme under the Marie Curie Skłodowska-Curie grant agreement No. 642294. M.B.-P. received funding from Agence Nationale de la Recherche through grant No. ANR-18-CE29-0012 (Photochromics project).

Acknowledgments: We acknowledge the financial support of the ITN-EJD-TCCM PhD Fellowship as part of the Marie Skłodowska-Curie Actions. This work was granted access to the HPC resources of CALMIP supercomputing center under the allocation 2019-[0880].

Conflicts of Interest: The authors declare no conflict of interest. The funders had no role in the design of the study; in the collection, analyses, or interpretation of data; in the writing of the manuscript, or in the decision to publish the results.

References

1. Woike, T.; Haussühl, S. Infrared-Spectroscopic and Differential Scanning Calorimetric Studies of the Two Light-Induced Metastable States in K₂[Ru(NO₂)₄(OH)(NO)]. *Solid State Commun.* **1993**, *86*, 333–337. [[CrossRef](#)]
2. Fomitchev, D.V.; Coppens, P. X-ray Diffraction Analysis of Geometry Changes upon Excitation: The Ground-State and Metastable-State Structures of K₂[Ru(NO₂)₄(OH)(NO)]. *Inorg. Chem.* **1996**, *35*, 7021–7026. [[CrossRef](#)] [[PubMed](#)]
3. Fomitchev, D.V.; Coppens, P.; Li, T.; Bagley, K.A.; Chen, L.; Richter-Addo, G.B. Photo-induced metastable linkage isomers of ruthenium nitrosyl porphyrins. *Chem. Commun.* **1999**, 2013–2014. [[CrossRef](#)]
4. Da Silva, S.C.; Franco, D.W. Metastable Excited State and Electronic Structure of [Ru(NH₃)₅NO]³⁺ and [Ru(NH₃)₄(OH)NO]²⁺. *Spectrochim. Acta A* **1999**, *55*, 1515–1525. [[CrossRef](#)]
5. Gorelsky, S.I.; Lever, A.B.P. Metastable States of Ruthenium (II) Nitrosyl Complexes and Comparison with [Fe(CN)₅NO]²⁻. *Int. J. Quantum Chem.* **2000**, *80*, 636–645. [[CrossRef](#)]
6. Ferlay, S.; Schmalte, H.W.; Francese, G.; Stoeckli-Evans, H.; Imlau, M.; Schaniel, D.; Woike, T. Light-Induced Metastable States in Oxalatenitrosylruthenium(II) and Terpyridinenitrosylruthenium(II) Complexes. *Inorg. Chem.* **2004**, *43*, 3500–3506. [[CrossRef](#)]
7. Schaniel, D.; Woike, T.; Boskovic, C.; Güdel, H.-U. Evidence for two light-induced metastable states in Cl₃[Ru(NH₃)₅NO]H₂O. *Chem. Phys. Lett.* **2004**, *390*, 347–351. [[CrossRef](#)]
8. Zangl, A.; Klüfers, P.; Schaniel, D.; Woike, T. Photoinduced Linkage Isomerism of {RuNO}⁶ Complexes with Biologands and Related Chelators. *Dalton Trans.* **2009**, *6*, 1034–1045. [[CrossRef](#)] [[PubMed](#)]

9. Schaniel, D.; Cormary, B.; Malfant, I.; Valade, L.; Woike, T.; Delley, B.; Krämer, K.W.; Güdel, H.-U. Photogeneration of Two Metastable NO Linkage Isomers with High Populations of up to 76% in trans-[RuCl(py)₄(NO)](PF₆)₂·1/2H₂O. *Phys. Chem. Chem. Phys.* **2007**, *9*, 3717–3724. [[CrossRef](#)]
10. Cormary, B.; Malfant, I.; Buron-Le Cointe, M.; Toupet, L.; Delley, B.; Schaniel, D.; Mockus, N.; Woike, T.; Fejfarová, K.; Petříček, V.; et al. [Ru(py)₄Cl(NO)](PF₆)₂·0.5H₂O: A Model System for Structural Determination and Ab Initio Calculations of Photo-Induced Linkage NO Isomers. *Acta Cryst. B* **2009**, *65*, 612–623. [[CrossRef](#)]
11. Cormary, B.; Ladeira, S.; Jacob, K.; Lacroix, P.G.; Woike, T.; Schaniel, D.; Malfant, I. Structural Influence on the Photochromic Response of a Series of Ruthenium Mononitrosyl Complexes. *Inorg. Chem.* **2012**, *51*, 7492–7501. [[CrossRef](#)] [[PubMed](#)]
12. Khadeeva, L.; Kaszub, W.; Lorenc, M.; Malfant, I.; Buron-Le Cointe, M. Two-Step Photon Absorption Driving the Chemical Reaction in the Model Ruthenium Nitrosyl System [Ru(py)₄Cl(NO)](PF₆)₂·1/2H₂O. *Inorg. Chem.* **2016**, *55*, 4117–4123. [[CrossRef](#)]
13. Tassé, M.; Mohammed, H.S.; Sabourdy, C.; Mallet-Ladeira, S.; Lacroix, P.G.; Malfant, I. Synthesis, Crystal Structure, Spectroscopic, and Photoreactive Properties of a Ruthenium(II)-Mononitrosyl Complex. *Polyhedron* **2016**, *119*, 350–358. [[CrossRef](#)]
14. Mikhailov, A.A.; Wenger, E.; Kostin, G.A.; Schaniel, D. Room-Temperature Photogeneration of Nitrosyl Linkage Isomers in Ruthenium Nitrosyl Complexes. *Chem. Eur. J.* **2019**, *25*, 7569–7574. [[CrossRef](#)] [[PubMed](#)]
15. Mikhailov, A.; Vuković, V.; Kijatkin, C.; Wenger, E.; Imlau, M.; Woike, T.; Kostin, G.A.; Schaniel, D. Combining Photoinduced Linkage Isomerism and Nonlinear Optical properties in Ruthenium Nitrosyl Complexes. *Acta Cryst.* **2019**, *B75*, 1152–1163. [[CrossRef](#)]
16. Ford, P.C.; Bourassa, J.; Miranda, K.; Lee, B.; Lorkovic, I.; Boggs, S.; Kudo, S.; Laverman, L. Photochemistry of Metal Nitrosyl Complexes. Delivery of Nitric Oxide to Biological Targets. *Coord. Chem. Rev.* **1998**, *171*, 185–202. [[CrossRef](#)]
17. Tfouni, E.; Krieger, M.; McGarvey, B.R.; Franco, D.W. Structure, Chemical and Photochemical Reactivity and Biological Activity of Some Ruthenium Amine Nitrosyl Complexes. *Coord. Chem. Rev.* **2003**, *236*, 57–69. [[CrossRef](#)]
18. Szundi, I.; Rose, M.J.; Sen, I.; Eroy-Reveles, A.A.; Mascharak, P.K.; Einarsdóttir, Ó. A New Approach for Studying Fast Biological Reactions Involving Nitric Oxide: Generation of NO Using Photolabile Ruthenium and Manganese NO Donors. *Photochem. Photobiol.* **2006**, *82*, 1377–1384. [[CrossRef](#)]
19. Bitterwolf, T.E. Photolysis of [Ru(bipy)₂(NO)Cl](PF₆)₂ in Frozen Ionic Glass Matrices. Evidence for Nitrosyl Linkage Isomerism and NO-Loss in a Physiologically Relevant Nitric Oxide Source. *Inorg. Chem. Commun.* **2008**, *11*, 772–773. [[CrossRef](#)]
20. Rose, M.J.; Mascharak, P.K. Photoactive Ruthenium Nitrosyls: Effects of Light and Potential Application as NO Donors. *Coord. Chem. Rev.* **2008**, *252*, 2093–2114. [[CrossRef](#)]
21. Rose, M.J.; Fry, N.L.; Marlow, R.; Hink, L.; Mascharak, P.K. Sensitization of Ruthenium Nitrosyls to Visible Light via Direct Coordination of the Dye Resorufin: Trackable NO Donors for Light-Triggered NO Delivery to Cellular Targets. *J. Am. Chem. Soc.* **2008**, *130*, 8834–8846. [[CrossRef](#)] [[PubMed](#)]
22. Giglmeier, H.; Kersch, T.; Klüfers, P.; Schaniel, D.; Woike, T. Nitric-Oxide Photorelease and Photoinduced Linkage Isomerism on Solid [Ru(NO)(terpy)(L)]BPh₄ (L = glycolate dianion). *Dalton Trans.* **2009**, 9113–9116. [[CrossRef](#)]
23. Ostrowski, A.D.; Ford, P.C. Metal Complexes as Photochemical Nitric Oxide Precursors: Potential Applications in the Treatment of Tumors. *Dalton Trans.* **2009**, 10660–10669. [[CrossRef](#)]
24. Fry, N.L.; Mascharak, P.K. Photoactive Ruthenium Nitrosyls as NO Donors: How to Sensitize Them toward Visible Light. *Acc. Chem. Res.* **2011**, *44*, 289–298. [[CrossRef](#)]
25. Akl, J.; Sasaki, I.; Lacroix, P.G.; Malfant, I.; Mallet-Ladeira, S.; Vicendo, P.; Farfán, N.; Santillan, R. Comparative Photo-Release of Nitric Oxide from Isomers of Substituted Terpyridinenitrosyl-Ruthenium(II) Complexes: Experimental and Computational Investigations. *Dalton Trans.* **2014**, *43*, 12721–12733. [[CrossRef](#)]
26. deBoer, T.R.; Mascharak, P.K. Recent Progress in Photoinduced NO Delivery with Designed Ruthenium Nitrosyl Complexes. *Adv. Inorg. Chem.* **2015**, *67*, 145–170.
27. Enriquez-Cabrera, A.; Sasaki, I.; Bukhanko, V.; Tassé, M.; Mallet-Ladeira, S.; Lacroix, P.G.; Barba-Barba, R.M.; Ramos-Ortiz, G.; Farfán, N.; Voitenko, Z.; et al. Replacing Two Chlorido Ligands by a Bipyridine Ligand in Ruthenium Nitrosyl Complexes with NO-Release Capabilities: A Comparative Study. *Eur. J. Inorg. Chem.* **2017**, 1446–1456. [[CrossRef](#)]

28. Amabilino, S.; Tassé, M.; Lacroix, P.G.; Mallet-Ladeira, S.; Pimienta, V.; Akl, I.; Sasaki, I.; Malfant, I. Photorelease of Nitric Oxide (NO) on Ruthenium Nitrosyl Complexes with Phenyl Substituted Terpyridines. *New J. Chem.* **2017**, *41*, 7371–7383. [[CrossRef](#)]
29. Enriquez-Cabrera, A.; Lacroix, P.G.; Sasaki, I.; Mallet-Ladeira, S.; Farfán, N.; Barba-Barba, R.M.; Ramos-Ortiz, G.; Malfant, I. Comparison of Carbazole and Fluorene Donating Effects on the Two-Photon Absorption and Nitric Oxide Photorelease Capabilities of a Ruthenium-Nitrosyl Complex. *Eur. J. Inorg. Chem.* **2018**, 531–543. [[CrossRef](#)]
30. Roose, M.; Tassé, M.; Lacroix, P.G.; Malfant, I. Nitric Oxide (NO) Photo-Release in a Series of Ruthenium-Nitrosyl Complexes: New Experimental Insights in the Search for a Comprehensive Mechanism. *New J. Chem.* **2019**, *43*, 755–767. [[CrossRef](#)]
31. Mai, S.; González, L. Molecular Photochemistry: Recent Developments in Theory. *Angew. Chem. Int. Ed.* **2020**. [[CrossRef](#)]
32. Kutateladze, A.G. *Computational Methods in Photochemistry*; CRC Press: Boca Raton, FL, USA, 2005.
33. Olivucci, M. *Computational Photochemistry*; Elsevier: Amsterdam, The Netherlands, 2005.
34. Garavelli, M. Computational Organic Photochemistry: Strategy, Achievements and Perspectives. *Theor. Chem. Acc.* **2006**, *116*, 87–105. [[CrossRef](#)]
35. Robb, M.A. *Theoretical Chemistry for Electronic Excited States*; Theoretical and Computational Chemistry Series; The Royal Society of Chemistry: London, UK, 2018. [[CrossRef](#)]
36. Daniel, C.; Gourlaouen, C. Chemical Bonding Alteration Upon Electronic Excitation in Transition Metal Complexes. *Coord. Chem. Rev.* **2017**, *344*, 131–149. [[CrossRef](#)]
37. Ciofini, I.; Daul, C.A.; Adamo, C. Phototriggered Linkage Isomerization in Ruthenium-Dimethylsulfoxide Complexes: Insights from Theory. *J. Phys. Chem. A* **2003**, *107*, 11182–11190. [[CrossRef](#)]
38. Göttle, A.J.; Dixon, I.M.; Alary, F.; Heully, J.-L.; Boggio-Pasqua, M. Adiabatic Versus Nonadiabatic Photoisomerization in Photochromic Ruthenium Sulfoxide Complexes: A Mechanistic Picture from Density Functional Theory Calculations. *J. Am. Chem. Soc.* **2011**, *133*, 9172–9174. [[CrossRef](#)]
39. Vieuxmaire, O.P.J.; Piau, R.E.; Alary, F.; Heully, J.-L.; Sutra, P.; Igau, A.; Boggio-Pasqua, M. Theoretical Investigation of Pphosphinidene Oxide Polypyridine Ruthenium(II) Complexes: Toward the Design of a New Class of Photochromic Compounds. *J. Phys. Chem. A* **2013**, *117*, 12821–12830. [[CrossRef](#)]
40. Göttle, A.J.; Alary, F.; Dixon, I.M.; Heully, J.-L.; Boggio-Pasqua, M. Unravelling the S→O Linkage Photoisomerization Mechanisms in *cis*- and *trans*-[Ru(bpy)₂(DMSO)₂]²⁺ Using Density Functional Theory. *Inorg. Chem.* **2014**, *53*, 6752–6760. [[CrossRef](#)]
41. Li, H.; Zhang, L.; Wang, Y.; Fan, X. Theoretical Studies on the Photoisomerization Mechanism of Osmium(II) Sulfoxide Complexes. *RSC Adv.* **2015**, *5*, 58580–58586. [[CrossRef](#)]
42. Li, H.; Zhang, L.; Zheng, I.; Li, X.; Fan, X.; Zhao, Y. Photoisomerization Mechanism of Ruthenium Sulfoxide Complexes: Role of the Metal-Centered Excited State in the Bond Rupture and Bond Construction Processes. *Chem. Eur. J.* **2016**, *22*, 14285–14292. [[CrossRef](#)]
43. Sanz García, J.; Alary, F.; Boggio-Pasqua, M.; Dixon, I.M.; Malfant, I.; Heully, J.-L. Establishing the Two-Photon Linkage Isomerization Mechanism in the Nitrosyl Complex *trans*-[RuCl(NO)(py)₄]²⁺ by DFT and TDDFT. *Inorg. Chem.* **2015**, *54*, 8310–8318. [[CrossRef](#)]
44. Sanz García, J.; Talotta, F.; Alary, F.; Dixon, I.M.; Heully, J.-L.; Boggio-Pasqua, M. A Theoretical Study of the N to O Linkage Photoisomerization Efficiency in a Series of Ruthenium Mononitrosyl Complexes. *Molecules* **2017**, *22*, 1667. [[CrossRef](#)] [[PubMed](#)]
45. Talotta, F.; Heully, J.-L.; Alary, F.; Dixon, I.M.; González, L.; Boggio-Pasqua, M. Linkage Photoisomerization Mechanism in a Photochromic Ruthenium Nitrosyl Complex: New Insights from an MS-CASPT2 Study. *J. Chem. Theory Comput.* **2017**, *13*, 6120–6130. [[CrossRef](#)] [[PubMed](#)]
46. Ignarro, L.J. *Nitric Oxide: Biology and Pathobiology*; Academic Press: San Diego, CA, USA, 2000.
47. Heilman, B.; Mascharak, P.K. Light-Triggered Nitric Oxide Delivery to Malignant Sites and Infection. *Phil. Trans. R. Soc. A* **2013**, *371*, 20120368. [[CrossRef](#)]
48. Sasaki, I.; Amabilino, S.; Mallet-Ladeira, S.; Tassé, M.; Sournia-Saquet, A.; Lacroix, P.G.; Malfant, I. Further Studies on the Photoreactivities of Ruthenium-Nitrosyl Complexes with Terpyridyl Ligands. *New J. Chem.* **2019**, *43*, 11241–11250. [[CrossRef](#)]
49. Freitag, L.; González, L. Theoretical Spectroscopy and Photodynamics of a Ruthenium Nitrosyl Complex. *Inorg. Chem.* **2014**, *53*, 6415–6426. [[CrossRef](#)]

50. Sanz García, J.; Alary, F.; Boggio-Pasqua, M.; Dixon, I.M.; Heully, J.-L. Is Photoisomerization Required for NO Photorelease in Ruthenium Nitrosyl Complexes? *J. Mol. Model.* **2016**, *22*, 284. [[CrossRef](#)]
51. de Lima Batista, A.P.; de Oliveira-Filho, A.G.S.; Galembeck, S.E. Photophysical Properties and the NO Photorelease Mechanism of a Ruthenium Nitrosyl Complex Investigated Using the CASSCF-in-DFT Embedding Approach. *Phys. Chem. Chem. Phys.* **2017**, *19*, 13860–13867. [[CrossRef](#)]
52. De Candia, A.G.; Marcolongo, J.P.; Etchenique, R.; Slep, L.D. Widely Differing Photochemical Behavior in Related Octahedral {Ru-NO}⁶ Compounds: Intramolecular Redox Isomerism of the Excited State Controlling the Photodelivery of NO. *Inorg. Chem.* **2010**, *49*, 6925–6930. [[CrossRef](#)]
53. Talotta, F.; Boggio-Pasqua, M.; González, L. Early Steps of the Ultrafast Photoisomerization Dynamics of *trans*-[RuCl(NO)(py)₄]²⁺. *Chem. Eur. J.* **2020**. [[CrossRef](#)]
54. Freitag, L.; Knecht, S.; Keller, S.F.; Delcey, M.G.; Aquilante, F.; Pedersen, T.B.; Lindh, R.; Reiher, M.; González, L. Orbital Entanglement and CASSCF Analysis of the Ru–NO Bond in a Ruthenium Nitrosyl Complex. *Phys. Chem. Chem. Phys.* **2015**, *17*, 14383–14392. [[CrossRef](#)]
55. Yanai, T.; Tew, D.P.; Handy, N.C. A New Hybrid Exchange–Correlation Functional using the Coulomb-Attenuating Method (CAM-B3LYP). *Chem. Phys. Lett.* **2004**, *393*, 51–57. [[CrossRef](#)]
56. Weigend, F.; Ahlrichs, R. Balanced Basis Sets of Split Valence, Triplet Zeta Valence and Quadruple Zeta Valence Quality for H to Rn: Design and Assessment of Accuracy. *Phys. Chem. Chem. Phys.* **2005**, *7*, 3297–3305. [[CrossRef](#)] [[PubMed](#)]
57. Andrae, D.; Häußermann, U.; Dolg, M.; Stoll, H.; Preuß, H. Energy-Adjusted Ab Initio Pseudopotentials for the Second and Third Row Transition Elements. *Theor. Chim. Acta* **1990**, *77*, 123–141. [[CrossRef](#)]
58. Granovsky, A.A. Extended Multi-Configuration Quasi-Degenerate Perturbation Theory: The New Approach to Multi-State Multi-Reference Perturbation Theory. *J. Chem. Phys.* **2011**, *134*, 214113. [[CrossRef](#)]
59. Galván, I.F.; Vacher, M.; Alavi, A.; Angeli, C.; Aquilante, F.; Autschbach, J.; Bao, J.J.; Bokarev, S.I.; Bogdanov, N.A.; Carlson, R.K.; et al. OpenMolcas: From Source Code to Insight. *J. Chem. Theory Comput.* **2019**, *15*, 5925–5964.
60. Roos, B.O.; Malmqvist, P.-Å.; Veryazov, V.; Widmark, P.-O. New Relativistic ANO Basis Sets for Transition Metal Atoms. *J. Phys. Chem. A* **2005**, *109*, 6575–6579. [[CrossRef](#)]
61. Roos, B.O.; Lindh, R.; Malmqvist, P.-Å.; Veryazov, V.; Widmark, P.-O. Main Group Atoms and Dimers Studied with a New Relativistic ANO Basis Set. *J. Phys. Chem. A* **2004**, *108*, 2851–2858. [[CrossRef](#)]
62. Ghigo, G.; Roos, B.O.; Malmqvist, P.-Å. A Modified Definition of the Zeroth-Order Hamiltonian in Multiconfigurational Perturbation Theory (CASPT2). *Chem. Phys. Lett.* **2004**, *396*, 142–149. [[CrossRef](#)]
63. Zobel, J.P.; Nogueira, J.J.; González, L. The IPEA Dilemma in CASPT2. *Chem. Sci.* **2017**, *8*, 1482–1499. [[CrossRef](#)]
64. Frisch, M.J.; Trucks, G.W.; Schlegel, H.B.; Scuseria, G.E.; Robb, M.A.; Cheeseman, J.R.; Scalmani, G.; Barone, V.; Petersson, G.A.; Nakatsuji, H.; et al. *Gaussian 09, Revision D.01*; Gaussian, Inc.: Wallingford, CT, USA, 2009.

Sample Availability: Samples of the compounds are not available from the authors.



© 2020 by the authors. Licensee MDPI, Basel, Switzerland. This article is an open access article distributed under the terms and conditions of the Creative Commons Attribution (CC BY) license (<http://creativecommons.org/licenses/by/4.0/>).